Ain Shams Engineering Journal (2016) 7, 543–552

Ain Shams University

Ain Shams Engineering Journal

www.elsevier.com/locate/asej
www.sciencedirect.com

CIVIL ENGINEERING

The effect of downstream curved edge on local scouring at 60 degree open channel junction using SSIIM1 model

Rasool Ghobadian [a,*], Mahsa Basiri [b]

[a] Water Engineering Department, Razi University, Kermanshah, Iran
[b] Former M.S. Student of Irrigation and Drainage, Water Engineering Department, Razi University, Kermanshah, Iran

Received 11 September 2014; revised 27 May 2015; accepted 1 June 2015
Available online 7 July 2015

KEYWORDS

Scouring depth;
Sedimentation bar;
Radius of curvature;
SSIIM1 model

Abstract Despite a large amount of research carried out on flow patterns in river confluences, only a few researches have focused on sediment transport. This research used 3D program (SSIIM 1) for calculating of local scouring and sedimentation at a 60 degree channel confluence. The model was tested by comparing with flow and sediment results of physical model. The results showed that the ability of model is relatively good to predict flow structure and position of the erosion and sedimentation pattern. The model was then applied to investigate the effect of downstream edge curvature with non-dimensional radius (r/w; r = radius of curvature, w = width of tributary channel) 0.25, 0.5, 0.75 and 1 with discharge ratio 0.5 and 0.66 on local scouring. The results showed that the reduction of scouring depth and sedimentation bar height for $r/w = 1$ comparing with sharp edge junction for discharge ratio 0.5 were 51% and 41% and for discharge ratio 0.66 were 28% and 19%.

1. Introduction

Confluences are important elements of every drainage network. As water moves through of a drainage network, it is forced to converge at confluences (Rhoads) [1]. Flow pattern at channel confluence which was first presented by Best [2] is shown in Fig. 1. Due to increasing of water discharge and collision of converging flows a complex three-dimensional and most highly turbulent location is occurred in the vicinity of the junction. Therefore a deep scour hole and point bar have developed in this area that cause the change in rivers morphology.

The use of numerical models for simulating the flow pattern in channel confluence has recently attracted the researcher's attention. Weerakoon and Tamia [3] focused on simple (rectangular and trapezoidal) channel. For simulation of flow structure they imposed a rigid lid solution, adopted a two-equation turbulence model and used a parabolic treatment. Weerakoon et al. [4] used a fully elliptic treatment in study of a 60 degree asymmetrical confluence. They found the predicted recirculation zone length in downstream direction was approximately

* Corresponding author. Tel.: +98 9188332489.
E-mail addresses: Rsghobadian@gmail.com (R. Ghobadian), basirimahsa@yahoo.com (M. Basiri).
Peer review under responsibility of Ain Shams University.

Production and hosting by Elsevier

http://dx.doi.org/10.1016/j.asej.2015.06.001

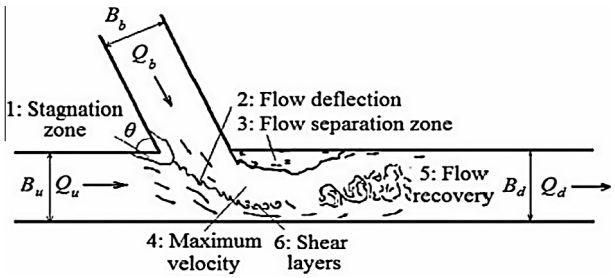

Fig. 1 Flow pattern in channel junction (Best, 1987).

30% too short. Bradbrook et al. [5,6] using of a modified form of $K-\varepsilon$ type turbulence model based upon RNG[1] theory investigated the influence of velocity ratio, confluence angle, level of confluence asymmetry and the degree of discordance on the magnitude of streamline curvature and the degree of topographic forcing. Their results on parallel confluence showed the negligible secondary circulation resulted with a depth ratio of 1 (concordance confluence). Also the results showed an asymmetry in secondary circulation may result in a symmetrical confluence due to velocity ratio effects. Lane et al. [7] with application of the model to the confluence of Kaskaskia River and Copper Slough, studied by Rhoads and Kenworthy [9,10] confirmed the helical circulation that formed resembled two back-to-back meanders. Bradbrook et al. [8] in order to explore the role of topography on flow structure compared model predictions for Kaskaskia River and Copper Slough confluence with the true bed topography and with the scour hole artificially filled in. They showed that above the scour hole there was a zone of negative dynamic pressure (i.e. where the pressure was lower than would be expected due to hydrostatic effect alone) even though the scour hole slope was too shallow for there to be flow separation. This was coincident with the zone of maximum down welling into the scour hole.

Biron et al. [11] used a three-dimensional model to examine mixing processes immediately downstream of confluence as well as further downstream in the mainstream. Simulations are presented for concordant and discordant laboratory junction and a field confluence for low and high flow conditions. Result showed that the effect of bed discordance is very apparent at a cross-section of a tracer over a distance of 5 channel widths is 30% for discordant bed but only 10% for concordant bed in laboratory simulation. Additionally, flow rate ratio does not affect the general trend described above. At natural confluence (confluence of Boyonne and Berthier rivers, Quebec, Canada) effect of bed discordance on flow mixing is more important at the low flow than at the high flow with corresponding decreases in the standard deviation of 31% and 18% over 3.5 channel widths.

Huang et al. [12] validated a three-dimensional model using the experimental data of a 90° junction flow under two conditions. In the first condition (RUN2) the discharges in upstream main channel and lateral channel were 0.043 and 0.127 m^3/s, respectively. For second condition (RUN5) they were 0.127 and 0.043 m^3/s, respectively. The total discharge was 0.17 m^3/s and downstream tail water was fixed at 0.296 m for both conditions. Good agreement was obtained between the model simulation and experimental measurement. Also, the effect of changing in junction angle (from 30° to 90°) on flow characteristics was investigated. It was founded that the size of separation zone and strength of secondary flow increase with junction angle. Ghobadian [13] carried out extensive studies on scour hole at river confluence. All of his tests were conducted for sharp edge confluence. His results showed that as the downstream Froude number, discharge ratio and the angle of river confluence increase, the scouring depth increases too. Also, as the channel width ratio increases or the sediment sizes increase, the scouring depth was reduced. Borghei and Sahebari [14] conducted an experimental study on the scour patterns at open channels confluence. They studied the effect of the angle between the two channel, discharge and width ratio of the tributary to the downstream channel branches on maximum scour hole depth. They found that the position of the maximum scouring depth moves to the outer wall and upstream to the main channel as effected by the dimensionless variables. They presented an equation for predicting scour depth. Bahramijovein and MandAkhtari [15] studied on flow structure in strongly curved bends at open channel 90-degree bends. Their experiments were conducted in a flume, 6 m long, 0.4 m wide, 0.45 m high and 0.6 m radius of center line of bend, made up of compacted plastic materials and different depths of flow (4.5, 6, 9, 12, 15 cm). Their results showed that the transverse slope of water surface in bends was not linear. Their aim was to predict depth of flow, position of maximum velocity and the place which must be protected from erosion in strongly curved bends. Liu et al. [16] carried out an experimental study on flow pattern and sediment transportation at a 90 degree open-channel confluence with different discharge ratios (q^*) of the tributary flow to the total flow. Mohamadi et al. [17] conducted an experimental study on local scour at curved edge of open-channel junctions. Their results showed that as the radius of curvature increases, the maximum local scour decreases significantly and the location of maximum scouring depth shifted downstream and toward the center of the main channel. They provide an equation for predicting the maximum scour depth.

Despite a large amount of experimental and numerical researches carried out on flow patterns at river confluences, only a few researches have focused on sediment transport. Most notably very little attention has been given to numerical simulation of the scour hole and point bar formation at river confluences. Therefore this paper uses a numerical simulation approach to predict the local scouring and sedimentation pattern at laboratory 60 degree channel confluences. Then the model was applied to investigate the effect of downstream curved edge with different non-dimensional radius (r/w) and discharge ratios on local scouring.

2. Method

2.1. Numerical model: theory and assumption

The current study used a finite volume CFD model (SSIIM1) to compute scouring depth and point bar height at 60 degree channel confluence. SSIIM1 program uses a finite volume method for discretization, together with the power-law scheme or the second order upwind scheme. The SIMPLE method is used for pressure coupling. An implicit solver is used to

[1] Re-Normalization Group.

produce velocity field in the geometry with a structured grid. The velocities are used when solving the convection-diffusion equations for different sediment size. This gives sediment erosion and deposition pattern.

The Navier-Stockes equations for turbulent flow in a general three-dimensional geometry are solved to obtain the water velocity:

$$\frac{\partial U_i}{\partial t} + U_j \frac{\partial U_i}{\partial x_j} = \frac{1}{\rho}\frac{\partial}{\partial x_j}(-P\delta_{ij} - \rho\overline{u_i u_j}), \quad j = 1,2,3 \tag{1}$$

where U = the average velocity, ρ = the density of water, P = pressure, δ_{ij} = the Kronecker delta, which is 1 if $i = j$ and 0 otherwise and x = general space dimension. The last term is Reynolds stress term, often modeled with the Boussinesq approximation:

$$\rho\overline{u_i u_j} = \rho\upsilon_t\left(\frac{\delta U_i}{\partial x_j} + \frac{\delta U_j}{\partial x_i}\right) - \frac{2}{3}\rho K\delta_{ij} \tag{2}$$

where υ_t is eddy viscosity and K is turbulent kinetic energy. **Eddy viscosity** is not a fluid property and depends strongly on the state of turbulence. **Eddy viscosity** can be determined by several model such as: zero-equation models, one-equation models and two-equation models as described in Rodi [18]. In two-equation models the eddy viscosity is a function of turbulent kinetic energy K and turbulent dissipation ε as described by Kolmogorov-Prandtl equation:

$$\upsilon_t = C'_\mu \frac{K^2}{\varepsilon} \tag{3}$$

Transport equation for K, that is similar for standard and RNG type of $K-\varepsilon$ turbulence model, is described as:

$$u_i\frac{\partial K}{\partial x_i} = \frac{\partial}{\partial x_i}\left(\frac{\upsilon_t}{\sigma_k}\frac{\partial K}{\partial x_i}\right) - \upsilon_t\left(\frac{\partial u_i}{\partial x_j} + \frac{\partial u_j}{\partial x_i}\right)\frac{\partial u_i}{\partial x_j} - \varepsilon \tag{4}$$

Similarly, the transport equation for ε is described by the following equation. In this equation there is an extra term representing the mean strain rates that accelerate the turbulent dissipation:

$$u_i\frac{\partial \varepsilon}{\partial x_i} = \frac{\partial}{\partial x_i}\left(\frac{\upsilon_t}{\sigma_\varepsilon}\frac{\partial \varepsilon}{\partial x_i}\right) - C_{1\varepsilon}\frac{\varepsilon}{K}P - C_{2\varepsilon}\frac{\varepsilon^2}{K} - \rho\alpha\frac{\varepsilon^2}{K} \tag{5}$$

The constants $C'_\mu, \sigma_k, \sigma_\varepsilon, C_{1\varepsilon}$ and $C_{2\varepsilon}$ are 0.09, 1, 1.3, 1.44 and 1.92 respectively. These are the default values in the SSIIM1 for $K-\varepsilon$ turbulence model. The extra term depends on a parameter α, which is determined by η, the ratio of time scales of turbulent strain to mean strain

$$\alpha = C'_\mu\eta^3\frac{(1-\eta/\eta_o)}{(1+\beta\eta^3)}, \eta = S\frac{K}{\varepsilon}, S = \sqrt{2S_{ij}^2} \quad \text{and } S_{ij} = 0.5\left(\frac{\partial u_i}{\partial x_j} + \frac{\partial u_j}{\partial x_i}\right) \tag{6, a-d}$$

In which η_o = fixed point for homogeneously strain turbulent flows (=4.8) and $\beta = 0.12$. When the mean strain is weak ($\eta \to 0$) the extra production term is small, but when the mean strain rate is strong (large η) the extra production term leads to an increase in turbulent dissipation. This results a decrease in eddy viscosity and therefore reduces momentum in the mean flow. The outcome of the accelerated turbulent dissipation is a computed recirculation zone which its size is comparable with those observed in the laboratory measurements.

Coupling of pressure and momentum equation is achieved by SIMPLE method (Patankar [19]) to find the pressure.

The suspended sediment transport was computed by solving the transient convection – diffusion equation for sediment concentration c:

$$\frac{\partial c}{\partial t} + U_j\frac{\partial c}{\partial x_j} + w\frac{\partial c}{\partial z} = \frac{\partial}{\partial x_j}\left(\Gamma\frac{\partial c}{\partial x_j}\right) \tag{7}$$

where c = concentration of sediment, w = fall velocity of the sediment particle, z = dimension in vertical direction, Γ = diffusion coefficient that was set to the eddy-viscosity taken from $K-\varepsilon$ model. The equation describes the transport of sediment, and includes the effect of the turbulence on reducing the setting velocity of the sediment and was solved on all cells except the cell closet to the bed, where the concentration in equilibrium situation was specified by Van Rijn's [20] equation:

$$c_{bed} = 0.015\frac{d}{a}\frac{\left(\frac{\tau-\tau_c}{\tau_c}\right)^{1.5}}{\left(d\left(\frac{(\rho_s-\rho_w)g}{\rho_w\upsilon^2}\right)^{1/3}\right)^{0.3}} \tag{8}$$

In which d = sediment particle diameter, a = Reference level, τ = bed shear stress, τ_c = critical bed shear stress for movement of sediment according to Shields curve, ρ_w and ρ_s = density of water and sediment, υ = viscosity of water and g = acceleration of gravity. After recommendation from Van Rijn's [20], a was set equal to the maximum value of half the bed-form height and the grain roughness of the bed. The sediment concentration was interpolated/extrapolated to the cell closest to the bed by using the Rouse [22] equation:

$$\frac{c_z}{c_{bed}} = \left(\frac{h-z}{z}\frac{a}{h-a}\right)^{\frac{w_s}{\beta K u^*}} \tag{9}$$

In which h = water depth; z = distance from the bed to the center of the bed cell; c_z = sediment concentration at z; c_{bed} = concentration of bed load; w_s = particle fall velocity of suspended sediment; β = coefficient related to diffusion of sediment particles; K = constant of Von Karman; and u^* = overall bed-shear velocity.

In addition to the suspended load, the bed load q_b was calculated. Van Rijn's [21] formula for bed load was used:

$$\frac{q_b}{d^{1.5}\sqrt{\frac{(\rho_s-\rho_w)g}{\rho_w}}} = 0.053\frac{\left[\frac{\tau-\tau_c}{\tau_c}\right]^{1.5}}{d^{0.3}\left[\left(\frac{(\rho_s-\rho_w)g}{\rho_w\upsilon^2}\right)\right]^{0.1}} \tag{10}$$

The bed level changes were computed by using the sediment continuity equation for the cells closest to the bed, called the bed cells. The total sediment continuity defect M (kg/s) in a bed cell was the sum of the sediment changes from the following processes: concentration changes over time, suspended sediment convection, particle fall velocity, suspended sediment diffusion and changes in bed load. The defect could be included into a continuity equation derived from Eq. (12) where also the bed load is added.

$$\rho_s\frac{\partial c}{\partial t} + \rho_s U_j\frac{\partial c}{\partial x_j} + \rho_s w\frac{\partial c}{\partial z} + \frac{\partial q_{b,x}}{\partial x} + \frac{\partial q_{b,y}}{\partial y} = \rho_s\frac{\partial}{\partial x_j}\left(\Gamma\frac{\partial c}{\partial x_j}\right) + \frac{\partial m}{\partial x_j}, \quad j = 1,2,3 \tag{11}$$

The bed load is here decomposed in two directions, x and y. To find m, the equation was integrated over each bed cell using the control volume method. The value of m was divided by the density of the sediments of the bed to find the volume of the deposits for each time step. This was then transformed into bed level changes for the grid. Both the sedimentation and the erosion processes were modeled using the same approach.

2.2. Boundary condition

2.2.1. Flow boundary condition

Boundary conditions for the Navier-Stokes equation are in many ways similar to the diffusion-convection equation, included boundary condition for inflow; outflow; water surface and bed/wall.

2.2.1.1. Inflow. Dirichlet boundary conditions have to be given at the inflow boundary. This is relatively straightforward to velocity. Usually it is more difficult to specify the turbulence. It is then possible to use a simple turbulence model ($\upsilon_t = 0.11$ $u^* h$ (Keefer [23]) or $\upsilon_t = 0.067 u^* h$ (depth average)) to specify the eddy viscosity. Given the velocity, it is also possible to estimate the shear stress (τ) at the entrance bed. Then the turbulent kinetic energy K at the inflow bed is determined by the following equation:

$$K = \frac{\tau}{\rho\sqrt{C'_\mu}} \tag{12}$$

Given the eddy viscosity and K at the bed equation $\left(\upsilon_t = C'_\mu \frac{K^2}{\varepsilon}\right)$ gives the value of ε at the bed. If K is assumed to vary linearly from the bed to the surface then Eq. (12) together with the profile of the eddy viscosity to calculate the vertical distribution of ε can be used.

2.2.1.2. Water surface. The free surface is computed using a fixed-lid approach, with zero gradients for all variables. The location of fixed lid and its movement as a function of time and the water flow field are computed by pressure and Bernoulli algorithm. The algorithm is based on pressure field. It uses the Bernoulli equation along the water surface to compute the water surface location based on fixed point that does not move (in this study downstream of confluence).

2.2.1.3. Bed/wall. The wall law for rough boundaries (Schlichting [24]) was used as a boundary condition for bed and wall:

$$\frac{U}{u^*} = \frac{1}{k} \ln\left(\frac{30y}{k_s}\right) \tag{13}$$

Here, the roughness is denoted k_s and in this study for the bed effective roughness according to Van Rijn equation is used, U and u^* = velocity and shear velocity, respectively, k is a coefficient equal to 0.4 and y = distance from the wall to the center of the cell.

2.2.2. Sediment boundary condition

The sediment concentration in equilibrium situation (Eq. (8)) for the cell closet to the bed was specified as bed boundary condition.

The other boundary conditions for the sediment concentration were a specified value at the upstream boundary and zero gradients for the water surface, the outlet, and the sides. However in this study only simulation of local scouring and sedimentation at confluence area is considered therefore no sediment feeding has done.

2.3. Experimental model

The experimental setup consists of a main flume 9 m long with 75 cm deep for the first 2 m and 45 cm for remaining 7 m and 35 cm wide, and a lateral flume 3 m long, 45 cm deep and 25 wide. Both flumes had a horizontal slope. At the upstream end of flumes stilling boxes were installed to reduce the kinetic energy of the entrance flow. A head tank provides a constant discharge to both stilling boxes. Discharge was measured by an electronic flow meter with an accuracy of 0.01 l/s. At the end of the main flume, a sluice gate controls the downstream water depth. Downstream water depth was measured at a location which has 0.5 m distance from the end gate. The lateral flume was connected to the main flume at 60 degree angle. Fig. 2 shows a plan view of the experimental setup.

An 11-cm layer of uniform sediment (D_{50} = 1.95 mm and $\sigma_g = \sqrt{D_{84}/D_{16}} = 1.28$) was laid on both channel beds. There was no sediment feeding or recirculation in these experiments. At the start of each run the flumes were filled slowly, keeping the tailwater gate closed. When the flow depth was high enough to avoid initial disturbances on the bed, the flow discharges were increased to the desired values and the tailwater gate was gradually opened until the desired flow depth was achieved. This situation was kept unchanged until the scour hole dimensions remained constant (5 hours for this case). At the end of the run the pump was shut down, the water was drained and the bed topography was measured using surveying equipment (point gauge). In order to measure the flow velocity, the bed of channel after scouring and sedimentation was fixed by a very thin layer of powder cement so that has not effect on bed roughness. Then the flow situation same before has established again. Table 1 shows the range of the relevant variables covered by the experiments. The Velocity vectors in vertical and main channel flow directions have measured by Laser Doppler Velocimeter (LDV) in several cross sections from 0.4 m upstream of downstream junction corner to 0.8 m downstream of it in a $10 \times 2.5 \times 2.5$ cm network (10 cm is in main channel flow direction).

2.4. Model application to channel confluence

Model application focused upon generation of an appropriate grid, and incorporation of the water surface, topography, sediment and inflow data. Grids have been shown to have a major effect upon model prediction and ideal grid would produce a flow field which is independent of grid dimensions, with as low as possible to save computational time and space. SSIIM 1 uses a structured method to generation of grid. In this study the mesh size in main channel is $131 \times 31 \times 12$ and lateral channel mesh size is $50 \times 21 \times 12$ longitudinal, transverse and vertical grid line. Grid independency test was informed and the mesh for main and lateral channel was the finest mesh. Then variation of maximum and minimum velocity, pressure, turbulent kinetic energy, scouring and sedimentation was

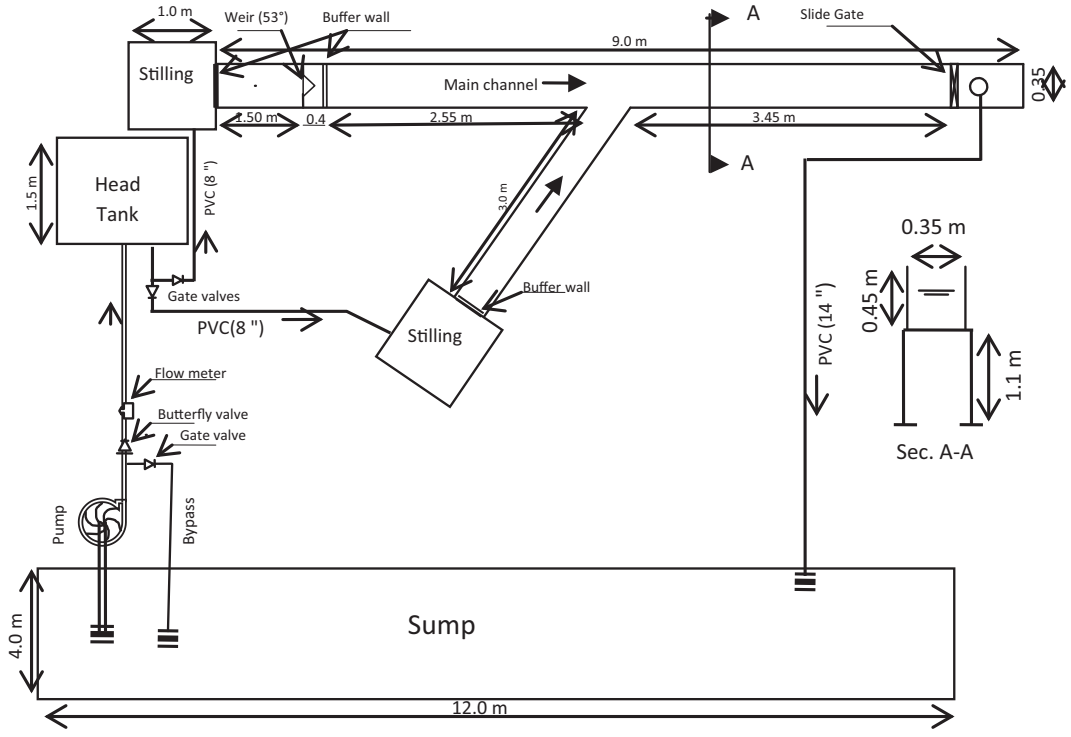

Fig. 2 Plan view of the experimental setup.

Table 1 Range of variables in this study.

Data	Main channel flow (L/s)	Lateral channel flow (L/s)	Discharge ratio	Tail water depth (cm)	Main channel bed width (cm)	Lateral channel bed width (cm)	Confluence angle (degree)	Grain size D_{50}(mm)
Flow simulation data	8.83	16.67	0.66	20	35	25	60	–
Sediment simulation data	10	10	0.5	12.76	35	25	60	1.95

compared. The small grids are near the bed. The experimental flow and sediment conditions (Table 1) were used as inlet condition for both the main and lateral channels. Total discharge (20 l/s) was used as outlet condition in the end of main channel where the water surface fixed in 12.76 cm from the bed. In experimental test the tailwater depth was measured at 0.5 m distance from the end gate. Finally 11 cm sediment thickness with D_{50} = 1.95 mm on bed of both the main and the lateral channel was defined as same as experimental test. Finally a time step 10 s was used. Also a power low scheme was used for the discretization of the convection terms. However the second order upwind method is also available in the model but use of this scheme for discretization of the convection terms causes divergence in solution even with changing at relaxation coefficient, reducing time step use of block-correction and changing the height of grid near the bed. The computation was stopped after 800 min because the significant change in scour hole dimension, sedimentation bar point dimension and also flow characteristic have not occurred. On the other hand experimental test also showed that bed level change was stopped after 5 h test running.

The mentioned model uses structured grid and with solving of Navier-Stokes and the standard turbulence model at the same time, simulates the flow and sediment at a junction of channels. A computer program to provide the required mesh was prepared. Fig. 3 shows the generated mesh for sharp and downstream curved edge junctions by mesh maker program.

3. Results

3.1. Calibration of model for flow

Before sediment pattern simulation, the model was first validated by comparing and analyzing the numerical simulation results of the flow pattern and the results of the experimental tests in a 60° junction of two straight channels were carried out by Ghobadian [13]. Longitudinal velocity profiles at different distances from the bed (z) in different cross sections of main channel were compared with the laboratory data in Fig. 4. It is indicated that the numerical model can simulate

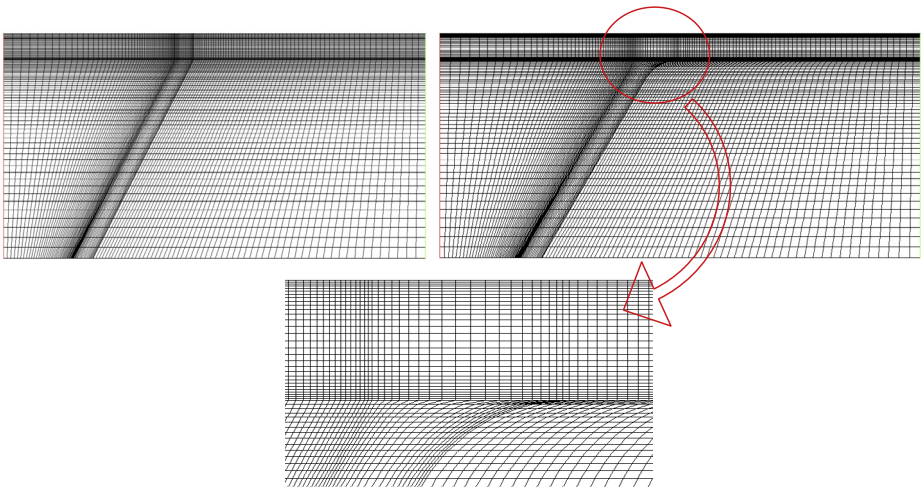

Fig. 3 View of sharp and curved downstream edge mesh.

the longitudinal velocities profiles with good accuracy. The main difference is in the area downstream of channel junction in vicinity of the separation zone. This difference could be due to the weakness of the $K-\varepsilon$ model of the simulation of flow in rotational zone. Weerakoon et al. [4] pointed that the $K-\varepsilon$ model had a weakness in predicted separation zone size less than the actual value. For quantitative evaluation the accuracy of the model the calculated longitudinal velocities values have

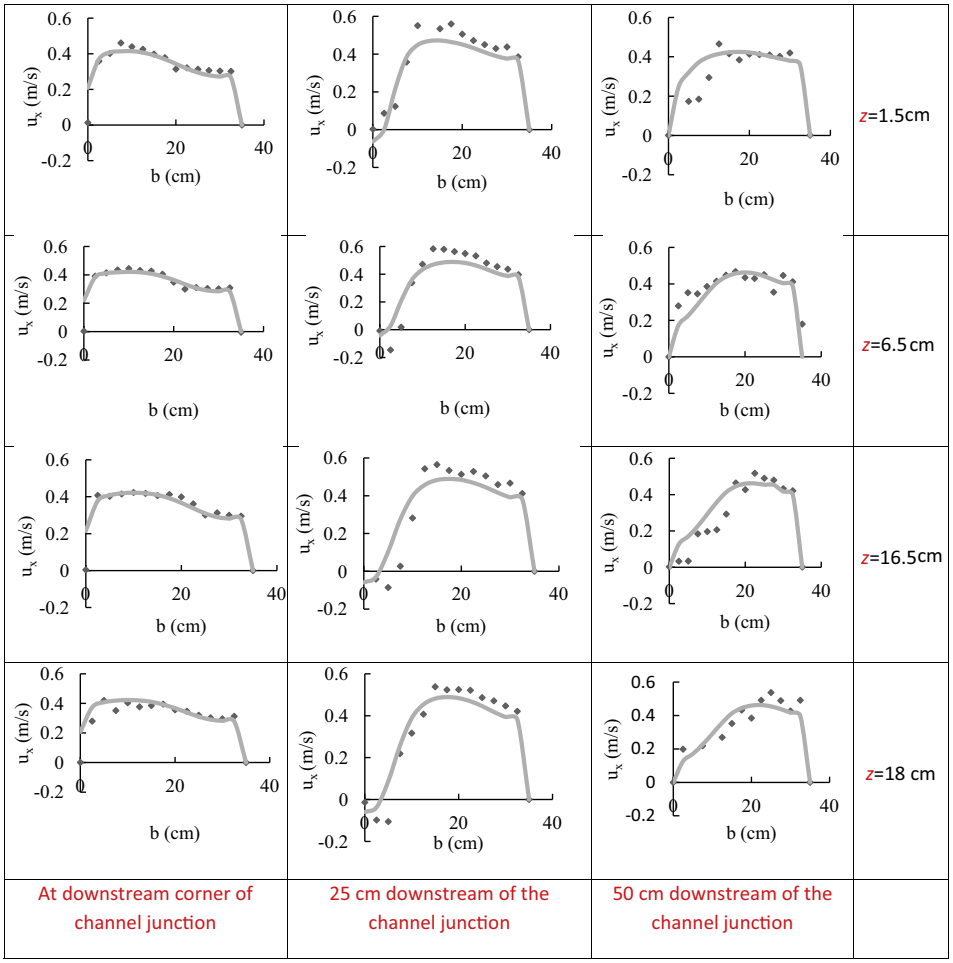

Fig. 4 Cross section longitudinal velocity profile at different distances from the bottom at different sections (points for experimental data and lines for simulation); u_x: longitudinal velocity, b: width of main channel, z: distance from the bottom.

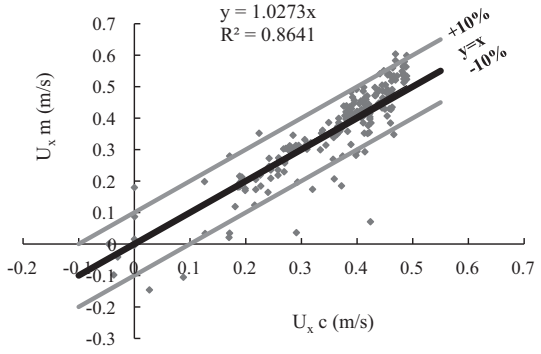

Fig. 5 Comparison of calculated and measured longitudinal velocities.

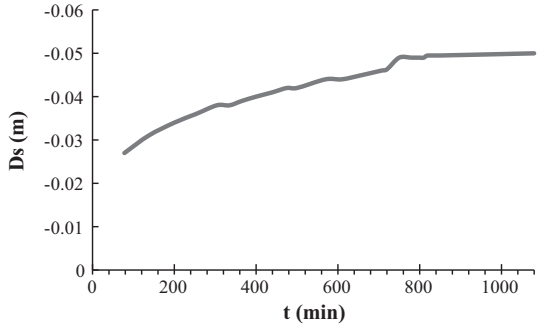

Fig. 6 The relationship between depth of local scouring and time for discharge ratio 0.5.

been plotted against the measured values and the results are presented in Fig. 5. As it can be seen from this figure most of data are between the 10% error bands. Several points that are below −10% they are in separation zone, where because of recirculation flow and weakness of the $K-\varepsilon$ model maximum error of flow pattern prediction occurred. Also the Root Mean Square Error was 0.061 m/s for longitudinal velocity. The coefficient of determination and slope of regression line were 0.864 and 1.027 respectively. This means that model

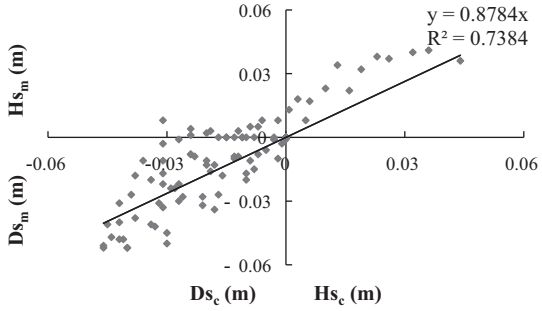

Fig. 8 Comparison of calculated and measured bed change (Ds = depth of scouring, Hs = sedimentation height).

can be applied for the prediction of flow pattern in river confluences.

3.2. Calibration of model for sedimentation

Scouring and sedimentation at river confluences is a recognized phenomenon that has reported by several researchers. Previous study showed that scouring and sedimentation pattern at river confluence is affected by discharge ratio, depth ratio, width ratio, confluence angle and also downstream densimetric Froude number (Ghobadian [13]). The model was calibrated using a set of experimental data on sedimentation adjacent to a 60° junction carried out by Ghobadian [13].

Scouring depth is a time related parameter and as it can be seen from Fig. 6 at the beginning of the simulation scour depth increases very fast and in continue the rate of increasing reduces to zero when the scour hole takes an equilibrium situation. No significant change in sedimentation and scouring pattern has been occurred during increasing the simulation time from 800 to 1000 min. It must be noted that for plotting Fig. 6 maximum scour depths calculated by the model have been used.

Fig. 7 shows the final scouring and sedimentation patterns calculated by the model and in the experimental test. It can be seen from this figure that the ability of model is relatively good to predict the position of the erosion and sedimentation patterns. However the values of maximum scour depth and

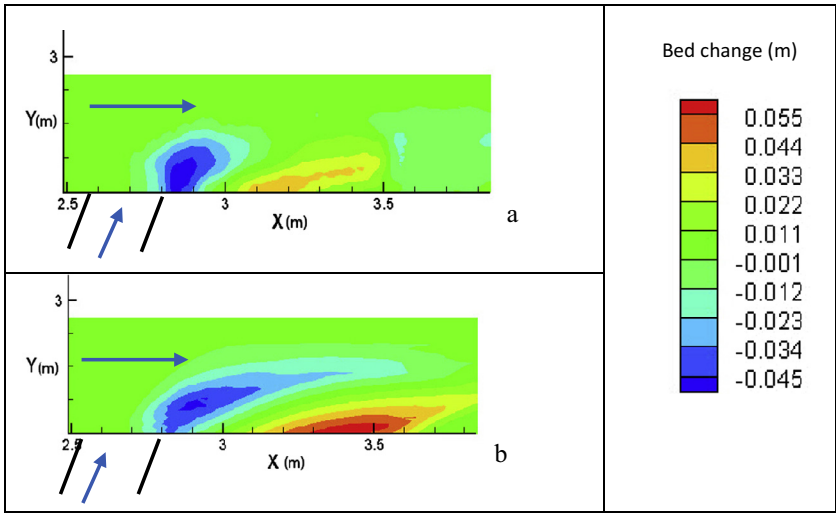

Fig. 7 Comparison of the scouring and sedimentation patterns for (a) experimental data (b) simulation.

sedimentation bar height have a little difference with the measured values. The values of maximum scour depth for experimental test and simulation are 0.052 and 0.047 m respectively. This difference could be due to the weakness of Van Rijn's equation to sediment transport and probably measured error. It must be noted that SSIIM1 only used the Van Rijn's equation for bed load transport. Also the result of simulation showed, similar to the experimental test no sediment transport occurred in tributary and main channel before the confluence.

In order to quantitative evaluation of the model accuracy, the calculated bed change values have been plotted against the measured values and the results are presented in Fig. 8. The coefficient of determination and slope of regression line were 0.738 and 0.878 respectively, which shows that the model is relatively good to predict bed change.

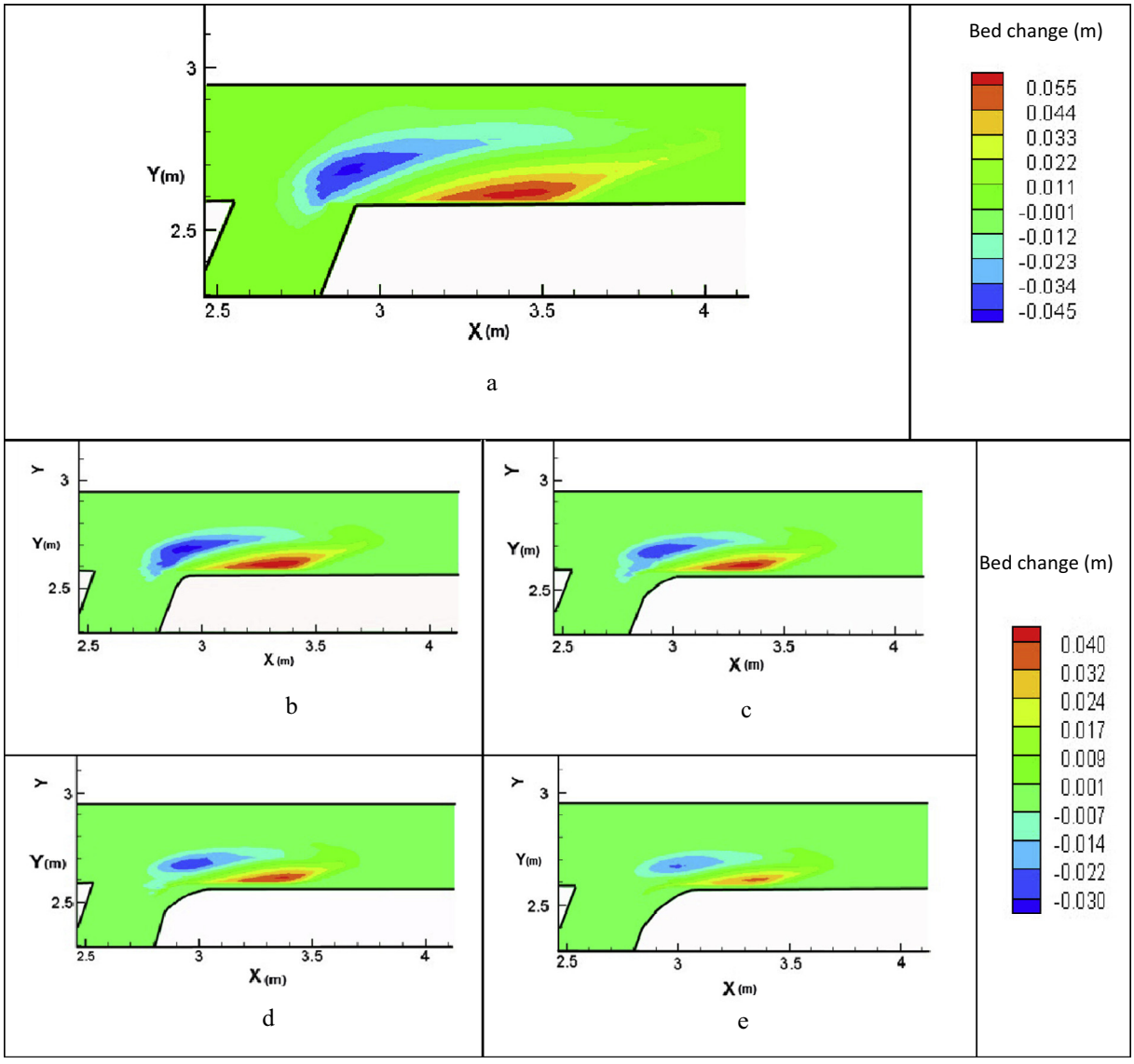

Fig. 9 The effect of curvature radius on scouring for discharge ratio 0.5 (a) sharp edge, (b) $r/w = 0.25$, (c) $r/w = 0.5$, (d) $r/w = 0.75$ and (e) $r/w = 1$.

Table 2 Position of points with maximum scouring depth and maximum sedimentation height.

Coordinate		Non-dimensional curvature radius				
		$r/w = 0$	$r/w = 0.25$	$r/w = 0.5$	$r/w = 0.75$	$r/w = 1$
Maximum scouring depth	X (m)	2.88	2.9	2.95	2.95	3
	Y (m)	2.68	2.69	2.67	2.67	2.67
Maximum deposition height	X (m)	3.41	3.31	3.35	3.35	3.33
	Y (m)	2.61	2.61	2.61	2.61	2.61

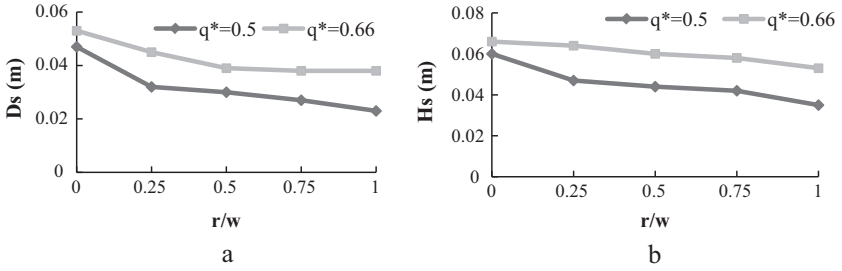

Fig. 10 The effect of curvature radius on (a) scouring and (b) sedimentation.

3.3. The effect of curvature of downstream edge on scouring

After calibrating the model, the effect of curvature of downstream edge on scouring and sedimentation pattern which was the main subject of the present research was investigated. The effect of non-dimensional curvature radius (r/w) 0.25, 0.5, 0.75 and 1 for discharge ratio 0.5 on scouring and sedimentation pattern is presented in Fig. 9, where it can be observed that with increasing curvature radius of junction, scouring depths and volume of scour hole decreases. As the scour hole becomes smaller, less sediment material is washed out and deposited further downstream creating the point bar therefore the sedimentation bar height and its volume reduce too. It should be defined that scouring depth and point bar height are directly related to separation zone dimension that limit the effective wide of main channel to pass combined flow. With increasing curvature radius of downstream edge of the junction, dimensions of flow separation zone which is created at downstream junction corner reduces. This is because as curvature radius of downstream edge increases, penetration of tributary channel flow into the main channel is reduced. Also as it can be observed from Fig. 9 values of maximum scouring depth for non-dimensional curvature radius (r/w) 0.25, 0.5, 0.75 and 1 are 0.032, 0.03, 0.027 and 0.023 m respectively. Comparing with the sharp edge, the reduction of maximum scouring depth was 51% for $r/w = 1$.

Table 2 shows the locations of the maximum scouring depth and sedimentation height for the discharge ratio of 0.5 and for various curvature radiuses. This table shows that, compared with those in sharp edge junctions, the longitudinal distance of the maximum scouring depth in the curved edge junctions has increased while, the width has remained almost constant. This means the location of the maximum scouring depth in the main channel has moved further downstream with not much change in its transverse direction. This table also shows the longitudinal distance of the maximum sedimentation height in curved edge junctions has decreased compared with those in sharp edge junctions. As a result, the longitudinal distance between the maximum scouring depth and sedimentation height has decreased in curved edge junctions compared with that in sharp edge junctions.

The variation of the scouring depth and sedimentation bar height for discharge ratio 0.5 and 0.66 with curvature radius is presented in Fig. 10, showing a decrease of bar height and scour depth with r/w. This can be explained again by the size of the separation zone, which is minimal for large curvature radius.

As it can be observed from Fig. 10a, for a certain r/w, scouring depth increases with discharge ratio. For example for $r/w = 1$ reduction of scouring depths for discharge ratios 0.5 and 0.66 was 51% and 28% respectively in comparison with the sharp edge junction. Also the maximum and minimum difference between scouring depths for discharge ratios 0.5 and 0.66 happened in $r/w = 1$ and $r/w = 0$ respectively. For discharge ratio 0.5, scouring depth decreases with increasing curvature radius with approximately uniform slope while for discharge ratio 0.66 from $r/w = 0$ to $r/w = 0.5$ scouring depth decrease then it remains relatively constant. This means for discharge ratio 0.5 and 0.66 optimum curvature radius are $r/w = 1$ and $r/w = 0.5$ respectively.

Fig. 10-b shows in comparison with the sharp edge junction, reduction of sedimentation bar height for $r/w = 1$ for discharge ratios 0.5 and 0.66 were 41% and 19% respectively. The minimum difference between sedimentation bar height for discharge ratio 0.5 and 0.66 happened in $r/w = 0$. However the difference between sedimentation bar height for discharge ratio 0.5 and 0.66 for the rest of non-dimensional curvature radius was almost equal.

4. Conclusions

In this paper using CFD model SSIIM1 flow and local scouring and sedimentation patterns at a 60 degree channel confluence were simulated and the model was calibrated. The result of model calibration showed that the model can be applied for the prediction of flow and scouring pattern in open channel junction. However the model accuracy for flow pattern simulation is higher than sediment pattern simulation. Then the model is applied to investigate the effect of curvature radius of downstream edge of the confluence with non-dimensional radius (r/w) 0.25, 0.5, 0.75 and 1 and discharge ratios 0.5 and 0.66 on local scouring. The results showed that with increasing radius of curvature scour depth and sedimentation bar height decreases. Reduction of scour depth for $r/w = 1$ and for discharge ratios 0.5 and 0.66 was 51% and 28% respectively in comparison with the sharp edge junction and reduction of sedimentation bar height was 41% and 19% respectively.

References

[1] Rhoads BL. Scaling of confluences dynamics in river systems: some general considerations. River Costal Estuarine Morphodyn 2005:379–87.

[2] Best JL. Flow dynamics at river channel confluences: implications for sediment transport and bed morphology. Recent Dev Fluvial Sedimentol 1987;39:27–35.

[3] Weerakoon S, Tamia N. Three – dimensional calculation of flow in river confluence using boundary fitted coordinates. J Hydrosci Hydraul Eng 1989;7:51–62.

[4] Weerakoon SB, Kawahara Y, Tamia N. Three dimensional flow structure in channel confluences of rectangular section. 24th Int Assoc Hydro-Environ Eng Res 1991:373–80.
[5] Bradbrook KF, Biron PM, Lane SN, Richards KS, Roy AG. Investigation of controls on secondary circulation in a simple confluence geometry using a three-dimensional numerical model. Hydrol. Process. 2000;12(8):1371–96.
[6] Bradbrook KF, Lane SN, Richards KS, Biron PM, Roy AG. Role of bed discordance at asymmetrical river confluences. J Hydr Eng 2001;127(5):351–68.
[7] Lane SN, Bradbrook KF, Richards KS, Biron PM, Roy AG. Secondary circulation cells in river channel confluences: measurement artefacts or coherent flow structures? Hydrol. Process. 2000;14(11–12):2047–71.
[8] Bradbrook KF, Lane SN, Richards KS. Numerical simulation of three-dimensional, time-averaged flow structure at river channel confluences. Water Resour. Res. 2000;36(9):2731–46.
[9] Rhoads BL, Kenworthy ST. Flow structure at an asymmetrical stream confluence. Geomorphology 1995;11(4):273–93.
[10] Rhoads BL, Kenworthy ST. Time-averaged flow structure in the central region of a stream confluence. Earth Surf. Proc. Land. 1998;23(2):171–91.
[11] Biron PM, Ramamurthy AS, Han S. Three-dimensional numerical modeling of mixing at river confluences. J Hydr Eng 2004;130(3):243–53.
[12] Huang J, Weber LJ, Lai YG. Three-dimensional numerical study of flows in open-channel junctions. J Hydr Eng 2002;128(3):268–80.
[13] Ghobadian R. Investigation of flow, scouring and sedimentation at river-channel confluences. PhD thesis, Shahidchamran University Iran; 2007.
[14] Borghei SM, Sahebari AJ. Local scour at open-channel junctions. J. Hydraul. Res. 2010;48(4):538–42.
[15] Bahrami Jovein E, MandAkhtari A. Experimental study on flow structure in strongly curved open channel 90-degree bends. In: International symposium on water management and hydraulic engineering; 2009.
[16] T-h Liu, Chen L, Fan Bl. Experimental study on flow pattern and sediment transportation at a 90° open-channel confluence. Int J Sedim Res 2012;27(2):178–87.
[17] Mohamadi S, Bejestan MS, Ghobadian R. Local scour at curved edge of open-channel junctions. Caspian J Appl Sci Res 2013;2(4):33–40.
[18] Rodi W. Turbulence models and their application in hydraulics. Int Assoc Hydraul Res Sec 1980.
[19] Patankar SV. Numer Heat Transf Fluid Flow 1980:116–522.
[20] Van Rijn LC. Sediment transport, part II: suspended load transport. J Hydraul Eng 1984;110(11):1613–41.
[21] Van Rijn LC. Sediment transport, part I: bead load transport. J Hydraul Eng 1984;110(11):1431–56.
[22] Rouse H. Modern conceptions of the mechanics of fluid turbulence. Trans Am Soc Civil Eng 1937;102(1):463–543.
[23] Keefer TN. The relation of turbulence to diffusion in open channel flows. Ph.D. thesis, Department of Civil Engineering. Colorado State University, USA; 1971.
[24] Schlichting H. Boundary-layer theory. New York: McGraw-Hill; 1979.

Rasool Ghobadian earned his BS degree in Irrigation and Engineering in 1997, from Shahid Chamran University, Ahvaz, Iran, with first ranking. He has earned his M.S. degree and his Ph.D degree in Hydraulic Structures Engineering from Shaid Chamran University of Ahvaz and Tehran University in 2000 and 2007 respectively. He is currently employing in Department of Water Engineering, Razi University, Kermanshah, Iran, as associate professor. His main research interests include numerical modeling of unsteady flow in irrigation network and river systems, design of Hydraulic Structure and River Engineering. He has published more than a hundred papers in these areas of expertise.

Mahsa Basiri earned her BS degree in Water Engineering in 2011, from Razi University, Kermanshah, Iran, and her M.S. degree in Irrigation and Drainage Engineering in 2014 from Razi University of Kermanshah, Iran. Her main research interests include simulation of 3D-Flow and sediment transport in open channel and she has published several papers in these areas of expertise.